Available online at www.sciencedirect.com
ScienceDirect
Journal of the European Ceramic Society 26 (2006) 3557–3565
www.elsevier.com/locate/jeurceramsoc

Corrosion of selected ceramic materials in hot gas environment

Marco Fritsch [a,*], Hagen Klemm [a], Matthias Herrmann [a], Bjoern Schenk [b]

[a] *Fraunhofer-Institut for Ceramic Materials and Sintered Materials, IKTS Dresden, Winterbergstr. 28, 01277 Dresden, Germany*
[b] *Honeywell Engines, System & Services, 111 S. 34th Street, Phoenix, AZ 85072-2181, USA*

Received 28 September 2005; received in revised form 10 January 2006; accepted 21 January 2006
Available online 24 March 2006

Abstract

The temperature dependence of the hot gas corrosion behaviour of various ceramic materials (Al_2O_3, ZrO_2 (Y-TZP), mullite, $ZrSiO_4$ and YAG) was investigated. The tests were performed in a high temperature burner rig at temperatures between 1200 °C and 1500 °C, a total pressure of 1 atm with a water vapour partial pressure of 0.24 atm, a gas flow velocity of 100 m/s and test times of about 130–300 h.

ZrO_2 (Y-TZP) showed absolutely no corrosion, however, a very high susceptibility to thermal shock and phase transformation was observed.

The other materials suffered degradation above 1300 °C. This was the consequence of the formation and evaporation of volatile hydroxides (e.g. $Si(OH)_4$ and $Al(OH)_3$). YAG showed a low corrosion rate and the formation of a protective surface layer. The corrosion susceptibility of these materials was found to be higher with increasing temperature.

Thermochemical calculations of the partial pressure of volatile species formed in reaction with water vapour, affirm the observed differences in corrosion behaviour.
© 2006 Elsevier Ltd. All rights reserved.

Keywords: Corrosion; Al_2O_3; Mullite; ZrO_2; YAG

1. Introduction

The main strategic goal for future generations of gas turbine engines is the increase of the thermal efficiency of the turbine. This can be obtained by an increase of the hot gas temperature in the turbine. However, simultaneously a decrease of the emissions is required. For that reason lean combustion concepts with a lower amount of cooling air are needed. This means that the rise in thermal loading of the turbine components cannot be compensated by additional cooling. The components in the hot gas path have to withstand higher material temperatures.

Oxide and non oxide ceramic materials are promising candidates for gas turbine components operating at elevated temperatures.[1] However, the common structural ceramics like SiC, Si_3N_4 and Al_2O_3 showed insufficient stability in high velocity combustion environments. Especially, water vapour in the combustion gas attacks the ceramic surface by the formation and evaporation of Si-hydroxides[2–5] (SiC, Si_3N_4) and Al-hydroxides[6,7] (Al_2O_3). Recession rates in the range of about 0.5–1 μm/h were observed for advanced Si_3N_4, SiC and Al_2O_3 materials destroying the materials after service in application relevant times (>10,000 h).[2–6] Therefore, the development of environmental barrier coatings (EBC) or material concepts, which have thermodynamic stability in hot gas environment, are needed. Oxide ceramics are promising candidates for environmental barrier coating systems, due to their natural stability in oxidative environments. However, a comprehensive understanding about the stability of these materials in hot gas environment is additional required.

In the present study the hot gas stability of various oxide ceramic materials will be presented.

2. Experimental

The corrosion behaviour of selected ceramics (Table 1) was investigated. Dense Al_2O_3 (AKP50 HC Stark), ZrO_2 (ZrO_2-TZP 3Y TOSOH), mullite (AKP50 HC Stark and SiO_2 Hereaus) and $ZrSiO_4$ (ZrO_2-TZP 3Y TOSOH and SiO_2 Hereaus) were fabricated by stoichiometric mixture of the starting powders and hot pressing at 1600 °C. YAG was fabricated by stoichiometric mixture of the starting powders (AKP50 and Y_2O_3 HC Stark) and hot pressing at 1700 °C. Bending bars were cut and ground

* Corresponding author. Tel.: +49 351 2553 869; fax: +49 351 2553 600.
E-mail address: marco.fritsch@ikts.fraunhofer.de (M. Fritsch).

0955-2219/$ – see front matter © 2006 Elsevier Ltd. All rights reserved.
doi:10.1016/j.jeurceramsoc.2006.01.015

Table 1
Summary of the materials investigated

Material	Composition	Densification	Density (g/cm^3)
α-Al_2O_3	α-Al_2O_3	Hot pressed	3.98
ZrO_2	ZrO_2 (Y-TZP incl. 3 mol.% Y_2O_3)	Hot pressed	6.00
Mullite	Al_2O_3, 28.2 wt.% SiO_2	Hot pressed	3.20
$ZrSiO_4$	ZrO_2 (Y-TZP incl. 3 mol.% Y_2O_3), 33 wt.% SiO_2	Hot pressed	4.23
YAG	$Y_3Al_5O_{12}$	Hot pressed	4.55

with a geometry of 3.8 mm × 3 mm × 36 mm as samples for the corrosion tests.

The corrosion tests were performed in a high temperature burner rig. The burner rig consisted of a combustor and a following test section. The inner walls of the combustor and the sample holder in the following test section consisted on SiC tubes with an inner diameter of 30 mm. Natural gas (mainly CH_4) was used as fuel for the combustor. To obtain a higher water vapour partial pressure in the combustion gas, water vapour was introduced separately to the air/fuel gas stream using an evaporator. The temperature was controlled by a Pt–Rh thermocouple near to the sample holder. A summary of the test conditions is given in Table 2.

The calculated composition of the combustion gas was obtained from the theoretical stoichiometric combustion equations and found to be in agreement to calculation performed with the computer program FactSage® (version 5.3.1). This computer program is based on the principle of minimizing the Gibbs free energy of the system.

To determine the influence of the temperature on the corrosion behaviour, it is important to keep other influencing factors, like the water vapour content, constant. Therefore the amount of added water steam to the gas flow was modified for each temperature.

The recession of the specimens was obtained by measuring the weight difference before and after the corrosion test. It is expressed by weight change ΔW (mg/cm^2) relating to the area of the test specimen exposed to the gas flow. From the weight chance ΔW with time the weight loss rate K_w (mg/cm^2 h) was determined. For linear corrosion kinetics the weight loss rate K_w can be calculated with a linear fit. The tests were conducted for 130–300 h at temperatures between 1200 and 1500 °C. The weight loss rate was calculated after reaching equilibrium conditions (after 30–50 h). The recession rate K_r (μm/h) gives information about the volume degradation and can be derived from the weight loss rate by using the density of the specimen.

Table 2
Summary of the test conditions

Definition	Symbol (units)	Value
Temperature	T (°C)	1200–1500
Gas flow velocity	v (m/s)	100
Total pressure	P (atm)	1
Test time for each temperature	t (h)	130–300
Calculated composition of the combustion gas		
Partialpressure of p_{H_2O}	p_{H_2O} (atm)	0.24
Partialpressure of p_{N_2}	p_{N_2} (atm)	0.64
Partialpressure of p_{O_2}	p_{O_2} (atm)	0.08
Partialpressure of p_{CO_2}	p_{CO_2} (atm)	0.04
Equivalence ratio	Φ	0.5–0.6 (fuel lean)

The activation energy was determined using the Arrhenius law. It was calculated with a linear fit between the weight loss rate K_w (logarithmic plot) and the temperature (inverse plot).

In order to specify the corrosion attack, the sample surfaces were analysed before and after the corrosion test by XRD. Based on these measurements the quantitative phase compositions were calculated with the computer program AutoQuan® (version 2.6.2.0). Information about microstructure alterations were obtained through observations of the sample surfaces and polished cross sections with element distributions of volatile species in the SEM.

Recession rate prediction was made based on the mass transfer theory of volatile species. The mass flux of volatile species under turbulent gas flow conditions can be obtained from the following formula[6]:

$$J \approx \frac{v^{4/5}}{P_{\text{total}}^{1/5}} \left(p_{H_2O}\right)^n \quad (1)$$

where J is the amount of mass transfer, v the gas flow velocity, P_{total} the system pressure, p_{H_2O} the water vapour partial pressure and n the water vapour partial pressure exponent.Under the test conditions of Table 2 ($v = 100$ m/s, $p_{H_2O} = 0.24$ atm and $P_{\text{total}} = 1$ atm) the evaluated data were fitted to the following formula:

$$K_w = a \exp\left(\frac{-E}{RT}\right) v^{4/5} \left(p_{H_2O}\right)^n (P_{\text{total}})^{-1/5} \quad (2)$$

where K_w is the weight loss rate (mg/cm^2 h), a a constant, E the activation energy (KJ/mol), R the general gas constant (8.31 J/mol K), T the temperature (K), v the gas flow velocity m/s), p_{H_2O} the water vapour partial pressure (atm), n the water vapour partial pressure exponent and P_{total} the system pressure (atm).

The FactSage® software package (version 5.3.1) was used for thermodynamic calculations and evaluation of the partial pressure of volatile species, formed by reaction with water vapour ($p_{H_2O} = 0.24$ atm, $P_{\text{total}} = 1$ atm). The thermodynamic data necessary for calculations were obtained from SGPS database (revised 2004) and Fact53 compound database (2004). For the YAG, YAM and Y_2SiO_5 phases a special data set of the System Y–Al–Si–C–O from SGTE[8] based on the data set of Groebner[9] was used. The data set for $Si(OH)_4$ was implemented from the literature.[10,11]

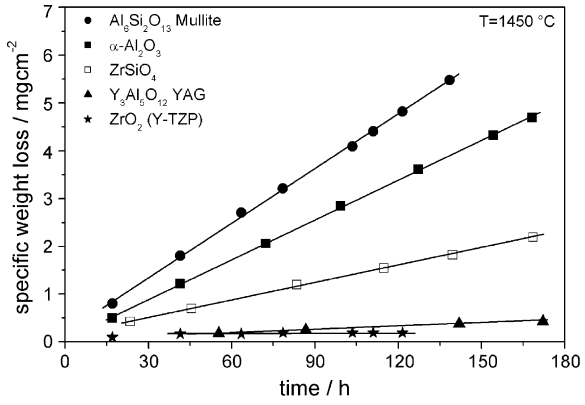

Fig. 1. Corrosion kinetic at 1450 °C.

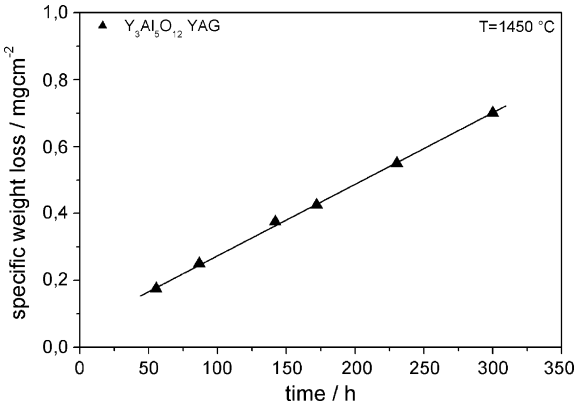

Fig. 2. Corrosion kinetic of YAG at 1450 °C.

3. Results and discussions

A summary of the corrosion test results is given in Table 3. Fig. 1 demonstrates the corrosion behaviour as weight loss as a function of time for the various ceramics at 1450 °C. Fig. 2 shows the corrosion kinetics of YAG for longer times.

A linear corrosion kinetics was found for Al_2O_3, mullite, $ZrSiO_4$ and YAG. This indicates a surface reaction controlled corrosion mechanism. YAG showed a significantly lower corrosion rate in comparison with the other ceramics. In the case of ZrO_2 (Y-TZP) hot gas corrosion was not found.

All samples showed at 1200 °C a very low corrosion rate, which is in the range of the uncertainty of the measurement. Therefore the calculation of the activation energy was restricted to the temperature range between 1300 and 1500 °C. Fig. 3 shows the Arrhenius plot of selected ceramics. ZrO_2 (Y-TZP) and $ZrSiO_4$ are left out, because ZrO_2 (Y-TZP) showed no detectable corrosion and $ZrSiO_4$ could not be manufactured in monophase. The derived activation energies from the Arrhenius relationship are summarized in Table 4.

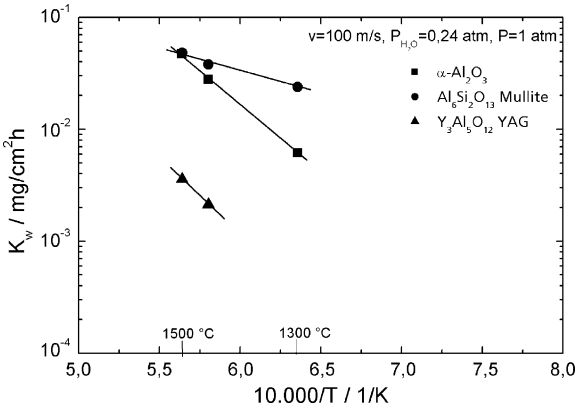

Fig. 3. Arrhenius plot of selected ceramics.

Table 5 shows the comparison of the crystalline surface phase compositions of the test samples before and after the corrosion test measured by XRD.

From the observed corrosion behaviour of the ceramics investigated, the corrosion reactions in Table 6 were deduced. Several

Table 3
Summary of corrosion test results of oxide ceramic materials

Material	T (°C)	Time (h)	Δm_t (mg)	K_w (mg/cm^2 h)	K_r (μm/h)	R^2 fit K_w
α-Al_2O_3	1200	131	–[a]	–	–	–
	1300	135	3.3	6.16×10^{-3}	1.55×10^{-2}	99.98
	1450	168	17.0	2.77×10^{-2}	6.96×10^{-2}	99.99
	1500	135	24.1	4.72×10^{-2}	1.19×10^{-1}	99.93
ZrO_2 (Y-TZP)	1200–1500		–	–	–	–
Mullite	1200	131	–	–	–	–
	1300	135	12.7	2.39×10^{-2}	7.47×10^{-2}	99.97
	1450	139	22.5	3.79×10^{-2}	1.18×10^{-1}	99.96
	1500	145	27.6	4.81×10^{-2}	1.50×10^{-1}	99.95
$ZrSiO_4$	1200	131	–	–	–	–
	1300	127	5.5	9.06×10^{-3}	2.14×10^{-2}	99.71
	1450	168	8.0	1.21×10^{-2}	2.86×10^{-2}	99.92
	1500	145	13.8	2.35×10^{-2}	5.56×10^{-2}	99.09
YAG	1200	131	–	–	–	–
	1300	135	–	–	–	–
	1450	300	2.8	2.12×10^{-3}	4.66×10^{-3}	99.91
	1500	145	2.1	3.58×10^{-3}	7.87×10^{-3}	97.98

[a] Results are within the uncertainty of the measurement.

Table 4
Activation energy

Material	ΔQ (kJ/mol)	R^2 fit ΔQ
α-Al_2O_3	233 ± 8	99.96
Mullite	78 ± 10	99.95
YAG	266	–

Table 5
Phase composition of the surface before and after hot gas exposure

Material	Phase composition after manufacturing (wt.%)	Phase composition of surface after hot gas corrosion (wt.%)
α-Al_2O_3	100 α-Al_2O_3	100 α-Al_2O_3
ZrO_2 (Y-TZP)	100 *t,c*-ZrO_2	32 *t,c*-ZrO_2 + 68 *m*-ZrO_2
Mullite	100 $Al_6Si_2O_{13}$	70 $Al_6Si_2O_{13}$ + 30 α-Al_2O_3
$ZrSiO_4$	73 $ZrSiO_4$ + 25 *t,c*-ZrO_2 + 2 SiO_2	32 *t,c*-ZrO_2 + 68 *m*-ZrO_2
YAG	100 $Y_3Al_5O_{12}$	49 $Y_3Al_5O_{12}$ + 18 $Y_4Al_2O_9$ + 33 Y_2SiO_5

studies show that under combustion atmospheres with a high water vapour content, the predominant volatile hydroxide for alumina is $Al(OH)_3$[6,7] and for SiO_2 is $Si(OH)_4$.[2] This is consistent with our thermochemical calculations.

Fig. 4 summarises the calculated partial pressures of the volatile species for each material and various temperatures for $P_{H_2O} = 0.24$ atm and $P_{total} = 1$ atm. Even if the calculations of the partial pressure of volatile species represent the thermodynamic equilibrium, which is maybe even locally not achieved under test conditions (due to the gas flow), the calculated ranking of the different ceramics is in agreement with the corrosion results.

Recession rate prediction was made based on Eq. (2). For Al_2O_3, mullite and YAG the following weight loss rate formulas were derived:

$$K_{w,Al_2O_3} = 6.96 \times 10^4 \exp\left(\frac{-233}{RT}\right) v^{4/5} \left(p_{H_2O}\right)^{1.5} (P_{total})^{-1/5} \quad (14)$$

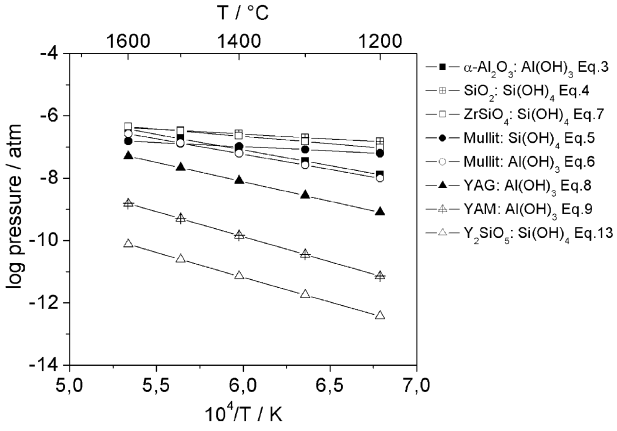

Fig. 4. Calculated partial pressure of volatile species $Si(OH)_4$ and $Al(OH)_3$ over different solid phases at a total pressure of 1 atm and a partial pressure of water vapour of 0.24 atm.

$$K_{w,Mullite} = 3.72 \exp\left(\frac{-78}{RT}\right) v^{4/5} \left(p_{H_2O}\right)^{2} (P_{total})^{-1/5} \quad (15)$$

$$K_{w,YAG} = 5.00 \times 10^4 \exp\left(\frac{-266}{RT}\right) v^{4/5} \left(p_{H_2O}\right)^{1.5} (P_{total})^{-1/5} \quad (16)$$

where K_w is the weight loss rate (mg/cm^2 h), the first number the fit constant a, R the general gas constant (8.31 J/mol K), v the gas flow velocity (m/s), p_{H_2O} the water vapour partial pressure (atm) and P_{total} the total system pressure (atm). For Al_2O_3 the water vapour exponent is 1.5 according to the theoretical formation of volatile hydroxide alumina (Eq. (3)). For mullite the water vapour exponent should lie within 1.5–2 according to the formation of Si-hydroxide (Eq. (5)) and Al-hydroxide (Eq. (6)). In Eq. (15), the exponent is assumed to be 2, because mullite suffers degradation mainly caused by silica volatilisation. For YAG the water vapour exponent should be 1.5 according to the formation of Al-hydroxide (Eq. (8)).

Fig. 5 shows the recession rate prediction for Al_2O_3, mullite and YAG under gas turbine conditions ($v = 150$ m/s, $P_{total} = 15$ atm, $P_{H_2O} = 1.5$ atm) for various temperatures and

Table 6
Proposed corrosion reactions with water vapour

Material	Corrosion reaction		$\Delta G^\circ_{1450\,^\circ C}$ (kJ)
α-Al_2O_3	$0.5Al_2O_3(s) + 1.5H_2O(g) \leftrightarrow Al(OH)_3(g)$	(3)	196.72
(SiO_2)	$SiO_2(s) + 2H_2O(g) \leftrightarrow Si(OH)_4(g)$	(4)	174.20
ZrO_2	–		–
Mullite	$0.5Al_6Si_2O_{13}(s) + 2H_2O(g) \leftrightarrow Si(OH)_4(g) + 1.5Al_2O_3(s)$	(5)	187.83
	$0.167Al_6Si_2O_{13}(s) + 1.5H_2O(g) \leftrightarrow Al(OH)_3(g) + 0.33SiO_2(s)$	(6)	201.65
$ZrSiO_4$	$ZrSiO_4(s) + 2H_2O(g) \leftrightarrow ZrO_2(tet, s) + Si(OH)_4(g)$	(7)	175.61
YAG	$0.286Y_3Al_5O_{12}[YAG](s) + 1.5H_2O(g) \leftrightarrow Al(OH)_3(g) + 0.214Y_4Al_2O_9(s)[YAM]$	(8)	245.62
	$0.5Y_4Al_2O_9[YAM](s) + 1.5H_2O(g) \leftrightarrow Al(OH)_3(g) + Y_2O_3(s)$	(9)	284.64
	$0.2Y_3Al_5O_{12}[YAG](s) + 0.3Si(OH)_4(g) + 0.9H_2O \leftrightarrow 0.3Y_2SiO_5(s) + Al(OH)_3(g) + H_2O(g)$	(10)	+150.31
	$0.5Y_4Al_2O_9[YAM](s) + Si(OH)_4(g) + Y_2SiO_5(s) + Al(OH)_3(g) + 0.5H_2O(g)$	(11)	−33.06
	$Y_2O_3(s) + Si(OH)_4(g) \leftrightarrow Y_2SiO_5(s) + 2H_2O(g)$	(12)	−317.70
(Y_2SiO_5)	$Y_2SiO_5(s) + 2H_2O(g) \leftrightarrow Si(OH)_4(g) + Y_2O_3(s)$	(13)	317.70

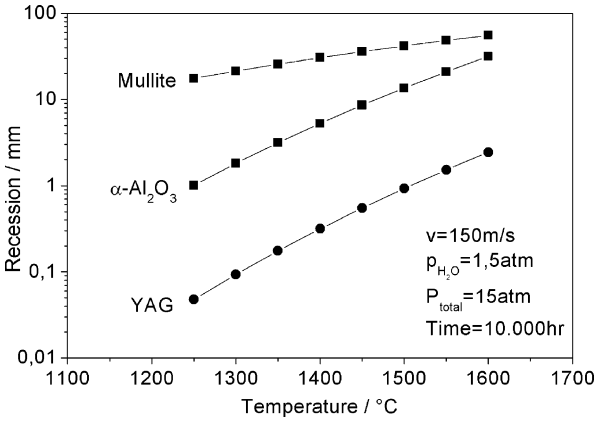

Fig. 5. Predicted recession under gas turbine conditions for various gas temperatures.

exposure time of 10,000 h. It is assumed that in a real gas turbine the flow velocity and the total pressure are higher compared to the test conditions in this study. The water vapour content is assumed to be 10% of the total pressure. Interpreting the recession data it should be considered, that the data for mullite and YAG might underestimate the real corrosion damage of the materials due to the formation of porous surface layers.

3.1. Corrosion of alumina

The weight loss rate of alumina shows a strong dependence with temperature in Fig. 3. The activation energy in Table 4 is comparable to other studies (Yuri et al.[6] 246 kJ/mol and Opila[7] 210 kJ/mol). The main corrosion reaction should be the formation of Al-hydroxides like $Al(OH)_3$ with water vapour from the combustion gas (Eq. (3)). Fig. 6 shows the surface of an alumina sample after corrosion at 1500 °C. Clearly the alumina grains can be seen, suggesting surface etching. It is plausible that the water vapour favours the attack of the grain boundaries, due to segregation and accumulation of impurities in them or simply to the less stable atomic bonding. Furthermore, it can be suggested that whole grains of alumina can fall out, if the cohesion of the grains becomes insufficient. The cross section of the alumina sample showed no corrosion layer. That agrees with the linear corrosion kinetics found for alumina in this study.

Recession rate prediction for alumina in Fig. 5 shows that under gas turbine conditions at elevated temperature between 1300 and 1600 °C the recession within 10,000 h lay between 1.8 and 32 mm. That will be too high for a structural gas turbine component. Therefore, alumina needs to be protected with EBC against corrosion.

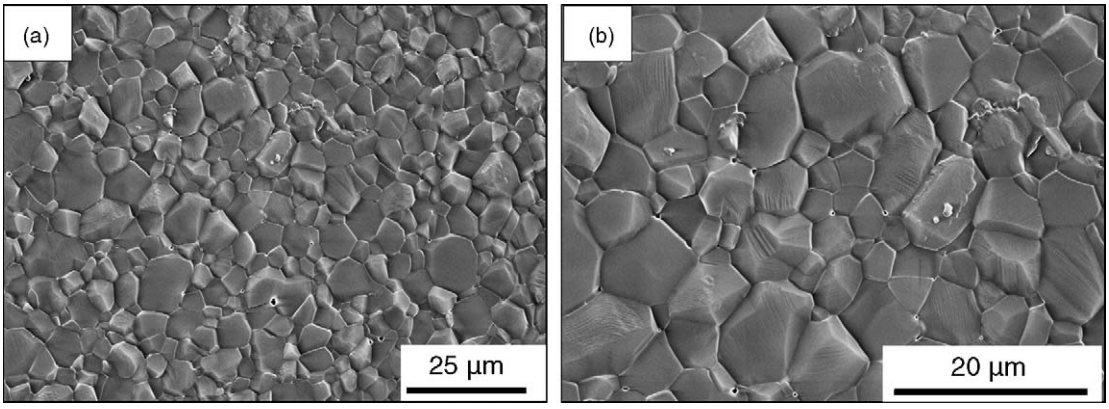

Fig. 6. Surface of Al_2O_3 (a and b) after corrosion at 1500 °C.

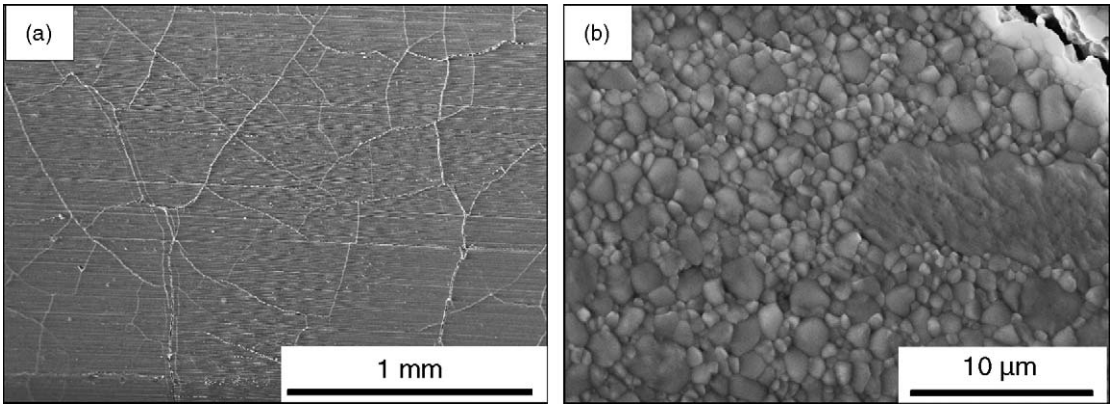

Fig. 7. Surface of ZrO_2 (Y-TZP) (a and b) after corrosion at 1450 °C.

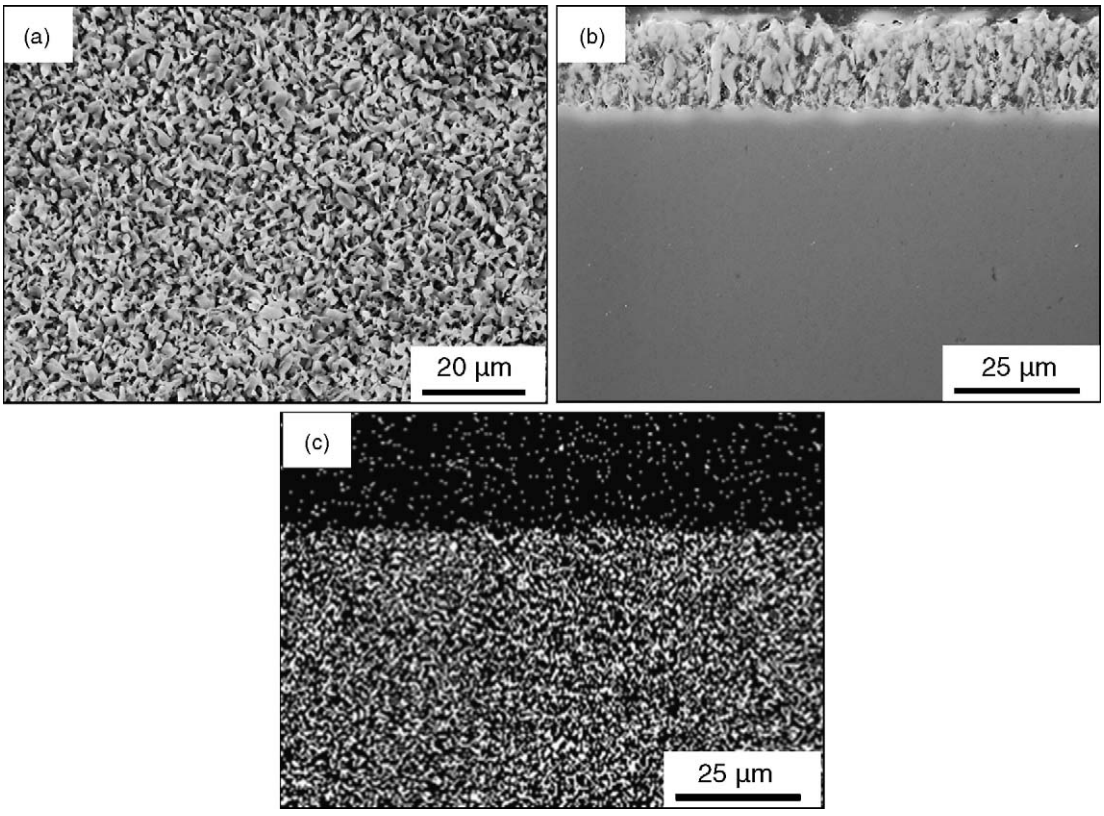

Fig. 8. Surface (a) and polished cross section (b) of mullite after corrosion at 1500 °C, EDX map of Si (c) from the cross section.

3.2. Corrosion of ZrO_2 (Y-TZP)

ZrO_2 (Y-TZP) showed absolutely no weight loss above the uncertainty of the measurement in the temperature range between 1200 and 1500 °C. Fig. 7 shows the surface of a ZrO_2 (Y-TZP) sample after corrosion at 1450 °C. Various cracks and grinding marks consulting from the manufacturing of the bending bar are visible. XRD observations of the sample surface after manufacturing revealed that, beside the tetragonal phase, cubic ZrO_2 was present. Because these two phases overlap each other in the XRD pattern, an explicit determination is difficult, and as a consequence they are listed in the Table 5 together. The corroded surface revealed that the initial tetragonal/cubic phase was destabilized. After the corrosion test a large amount of the monocline phase is observed. This transformation led to volume increase and subsequently to stress induced cracks. The transformation problem of ZrO_2 (Y-TZP) is well known in the literature.[12,13]

Due to its high corrosion stability, ZrO_2 (Y-TZP) is an EBC candidate, but the large mismatch in thermal expansion between ZrO_2 (Y-TZP) and structural ceramics like SiC, Si_3N_4 and Al_2O_3 make it difficult to use as a coating. As a consequence special focus has to be placed on thermal expansion and phase stability of ZrO_2 (Y-TZP) for use as an EBC material.

3.3. Corrosion of mullite

Mullite showed between 1300 and 1450 °C the highest weight loss rate among the investigated ceramics in the test. At 1500 °C, the weight loss rate equals the value of alumina. The XRD results of the corroded mullite surface (Fig. 8) are shown in Table 5. During corrosion, a porous layer of alumina was formed at the surface. EDX element distribution of Si in Fig. 8c, taken from the cross section of the corroded mullite sample (Fig. 8b), revealed that the Si leaches out of the surface with time. This means that the SiO_2 of the mullite reacts with the water vapour of the combustion gases. The reaction of SiO_2 with water vapour (Eq. (4)) is well documented in the literature.[2] The premier reaction should be the forming of volatile Si-hydroxides like $Si(OH)_4$ (Eq. (5)). An argument for this corrosion process is further the amount of the activity energy in Table 4. It is much lower than that of alumina, and comparable to that of Si-ceramics.[2,6] Nevertheless, it is assumed that concurrently small amounts of Al-hydroxide evaporate (Eq. (6)). The thermochemical calculations for mullite in Fig. 4 agree with the observed preferred volatility of $Si(OH)_4$ in comparison with $Al(OH)_3$. The partial pressure of $Si(OH)_4$ is higher than that of $Al(OH)_3$ up to 1500 °C.

The linear corrosion kinetics confirm that the developing porous corrosion layer on the surface does not protect the bulk material underneath from corrosion. The recession prediction in Fig. 5 showed that mullite has a higher recession rate than alumina and cannot be recommended as a material for EBC coatings.

3.4. Corrosion of $ZrSiO_4$

The XRD results in Table 5 revealed that the $ZrSiO_4$ sample was not obtained as a monophase material after manufacturing.

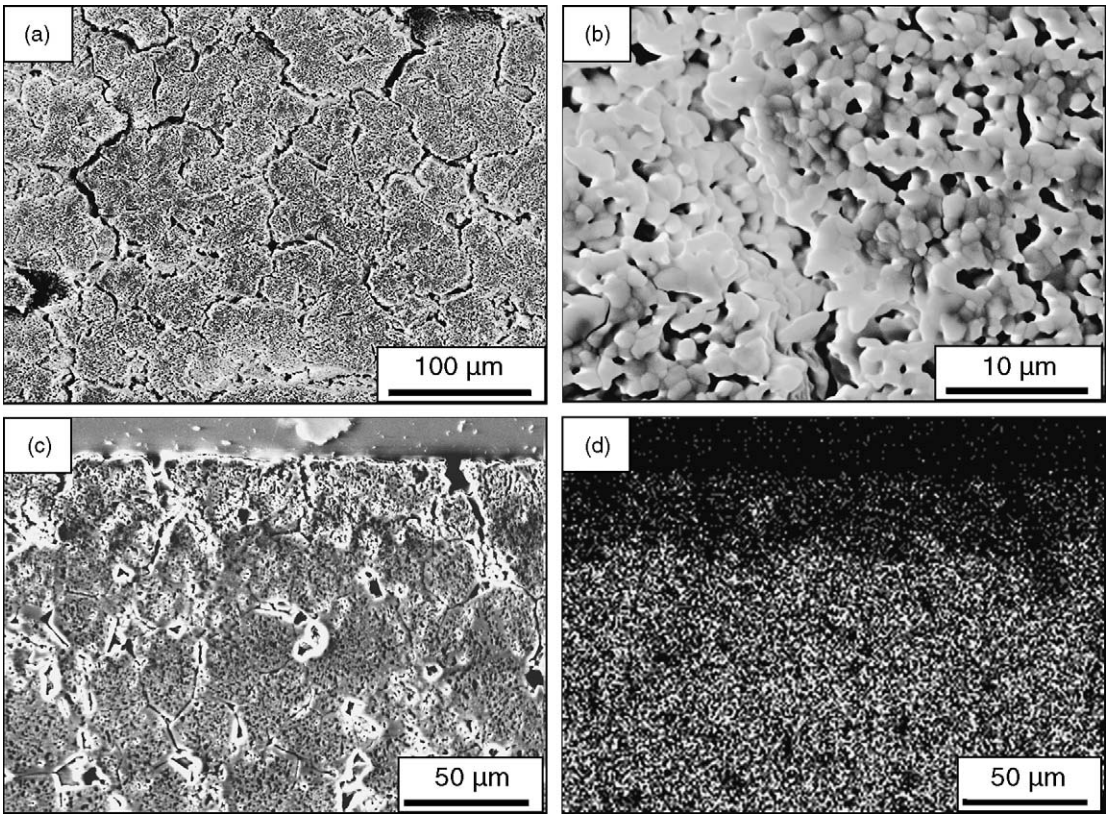

Fig. 9. Surface (a and b) and polished cross section (c) of $ZrSiO_4$ after corrosion at 1500 °C, EDX map of Si (d) from the cross section.

Beside $ZrSiO_4$ there was *t*,*c*-ZrO_2 and SiO_2 found in the bulk material. This showed that the stoichiometric mixture of the starting powders of *t*-ZrO_2 (Y-TZP) and SiO_2 did not react completely to form $ZrSiO_4$ under the given hot pressing conditions.

Fig. 9 shows the surface of the $ZrSiO_4$ after corrosion at 1500 °C. Remarkable cracks and spalling of the outer corrosion layer are visible. With XRD, *t*,*c*-ZrO_2 and *m*-ZrO_2 were found on the surface. Fig. 9d shows the element distribution of Si, taken from the cross section in Fig. 9c. It can be seen that Si is leached out of the surface, due to the chemical reaction to build volatile species. Based on these results two mean corrosion processes can be deducted. First SiO_2 from the $ZrSiO_4$ reacts with water vapour to yield volatile species which evaporate Eq. (7), so ZrO_2 is left. The monocline *m*-ZrO_2, found with XRD on the surface, belongs to the transformation of $ZrSiO_4$ to *m*-ZrO_2. This monocline *m*-ZrO_2 will transform into the tetragonal phase (or reverse) for every start and shut down of the burner rig. It is to be supposed that this volume change will cause stresses in the corrosion layer which can consequently lead to the crack formation observed. This means that the outer porous ZrO_2 layer gives little or no corrosion protection to the material underneath. Corresponding linear corrosion kinetics were observed. It is proposed that $ZrSiO_4$, even in monophase, is unstable in water vapour containing hot gas atmospheres and therefore not suitable for EBC coatings.

3.5. Corrosion of YAG

YAG showed over the complete temperature range a remarkably low weight loss rate in comparison to alumina and mullite. Nevertheless the recession increased with time. The activation energy derived from the Arrhenius plot in Fig. 3 is higher than that for alumina.

Fig. 10 shows the surface and the cross section of a YAG sample after corrosion at 1450 °C. The surface seems a little rough. The XRD observations of the corroded YAG surface in Table 5 show that, beside YAG, Y_2SiO_5 and $Y_4Al_2O_9$ (YAM) were formed during corrosion. The microstructure of a polished cross section in Fig. 10c and the element distributions of Al, Y and Si (Fig. 10d–f) taken from Fig. 10c affirm the existence of a surface layer. Especially the element distribution of Al shows that only the monosilicate layer was built on the surface. The YAM phase is assumed to be at the interphase between alumina and Y_2SiO_5. It is suggested that the YAG decomposed in contact with water vapour to YAM and Al-hydroxides (Eq. (8)). Further, the YAM can decompose in reaction with water vapour to form Y_2O_3 and Al-hydroxides (Eq. (9)). The existence of Si-hydroxides in the combustion gas, mainly from corrosion of the SiC tubes (sample holder), can lead to a simultaneous reaction of the Y_2O_3 with the Si-hydroxides to form Y_2SiO_5 (Eq. (12)). Further, $Si(OH)_4$ from the combustion atmosphere can be involved in the corrosion attack of YAG (Eq. (10)) or YAM (Eq. (11)). Nevertheless, the partial

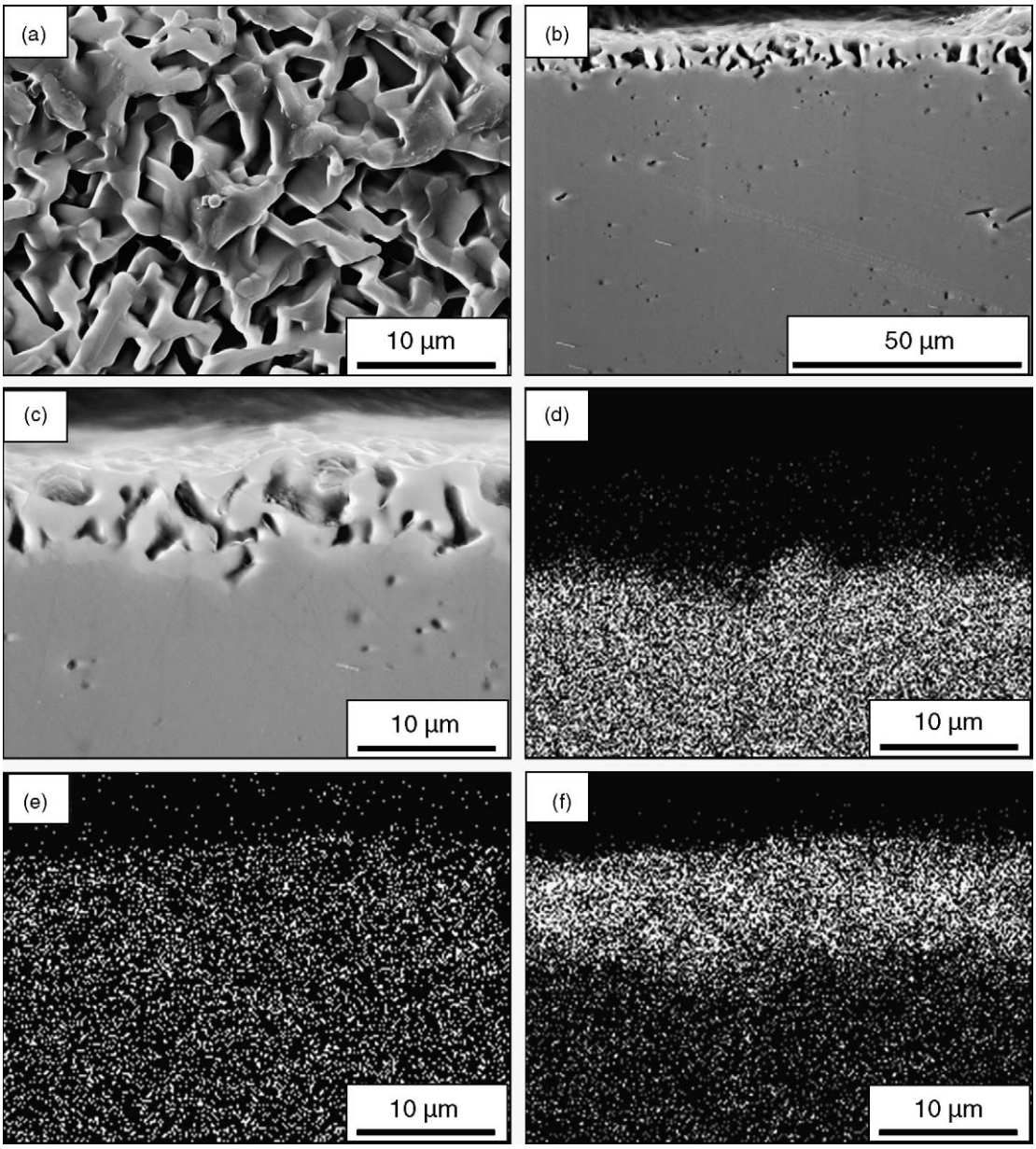

Fig. 10. Surface (a) and polished cross section (b and c) of YAG after corrosion at 1450 °C, XRD maps of Al (d), Y (e) and Si (f) from the cross section (c).

pressure of $Si(OH)_4$ in the combustion gas should be very low in comparison with the water vapour partial pressure. Therefore, the water vapour attack dominates the corrosion attack of YAG and the building of Al-hydroxides. The absorption of silica, in the form of Y_2SiO_5, on the surface led to a weight gain of the test specimen. It is proposed that in an atmosphere with no Si-hydroxides the weight loss rate of YAG should be higher.

The formation of Y_2SiO_5 under these environmental conditions confirms that rare earth monosilicates are very stable in hot gas environment.[14] Klemm et al.[15] and Ueno et al.[16] found monosilicates as corrosion layers on bulk disilicates. The detected YAM phase in Table 5 correspond to the decomposition of YAG into YAM and $Al(OH)_3$ (Eq. (8)). The observed higher environmental stability of the YAM and Y_2SiO_5 phases are in agreement with the calculated pressures of volatile hydroxides (Eqs. (9) and (13)) for these materials in Fig. 4.

Because a distinctive parabolic corrosion kinetic was not found (Fig. 2), it is proposed that the developing outer porous Y_2SiO_5 and YAM layer on the YAG surface has only a small protective influence of the bulk material underneath. The recession rate prediction in Fig. 5 shows for YAG an order of magnitude lower recession rates in comparison with alumina and mullite.

Further investigations are needed to clarify the corrosion behaviour of YAG. The results show, that water vapour led to corrosion attack of YAG and decomposition into YAM. Si-hydroxides from the combustion gas are involved in the corrosion reactions and led to a weight gain due to the building of Y_2SiO_5. It can be assumed that YAG will show in an atmosphere with no Si-hydroxides a higher corrosion rate.

4. Conclusions

The temperature dependence of the hot gas corrosion behaviour for various ceramic materials (Al_2O_3, ZrO_2 (Y-TZP), mullite, $ZrSiO_4$ and YAG) was investigated. Besides ZrO_2 (Y-TZP) all materials exhibited degradation above 1300 °C. This was the consequence of formation and evaporation of volatile hydroxides ($Si(OH)_4$ and $Al(OH)_3$). Al_2O_3, mullite and $ZrSiO_4$ showed at temperatures above 1300 °C a degradation that will be too high for environmental barrier coating applications. YAG showed a low corrosion coupled with the formation of a stable surface layer. ZrO_2 (Y-TZP) showed absolutely no corrosion, but is very susceptible to thermal shock and phase transformation.

All ceramics, beside ZrO_2 (Y-TZP), showed a strong increase in degradation with temperature. The thermochemical calculations are in agreement with the observed corrosion rates. If sufficient materials data are available, the theoretical calculation of the environmental stability of materials can be a tool for future EBC development.

References

1. Richerson, D. W., Ceramic components in gas turbine engines: Why has it taken so long? 28th International Conference on Advanced Ceramics and Composites. *Ceram. Eng. Sci. Proc.*, 2004, **25**(3), 3–32.
2. Opila, E. J., Oxidation and volatilization of silica formers in water vapor. *J. Am. Ceram. Soc.*, 2003, **86**(8), 1238–1248.
3. Yuri, L., Hisamatsu, T., Etori, Y. and Yamamoto, T., Degradation of silicon carbide in combustion gas flow at high temperature and speed. In *ASME Turbo Expo 2000*, 2000, ASME Paper 2000-GT-664.
4. Klemm, H., Corrosion of silicon nitride materials in gas turbine environment. *J. Eur. Ceram. Soc.*, 2002, **22**, 2735–2740.
5. Schenk, B., Strangman, T., Opila, E., Robinson, C., Fox, D., Klemm, H. *et al.*, Oxidation behavior of prospective silicon nitride materials for advanced microturbine applications. In *ASME Turbo Expo 2001*, 2001, ASME Paper 2000-GT-0459.
6. Yuri, I. and Hisamatsu, T., Recession rate prediction for ceramic materials in combustion gas flow. In *Proceedings of ASME Turbo Expo*, 2003, ASME Paper GT2003-38886.
7. Opila, E., Alumina volatility in water vapor at elevated temperatures. *J. Am. Ceram. Soc.*, 2004, **87**(9), 1701–1705.
8. 9288AOOS-SGTE Si–Y–Al–C–O Database. Scientific Group Thermodata, Europe, 2000.
9. Groebner, J., Constitution calculations in the system Y–Al–Si–C–O, Ph.D. thesis, University of Stuttgart, Germany, 1994.
10. Hashimoto, A., The effect of H_2O gas on volatilities of planet-forming major elements: I. Experimental determination of thermodynamic properties of Ca-, Al-, and Si-hydroxide gas molecules and its application to the solar nebula. *Geochim. Cosmochim. Acta*, 1992, **56**, 511–532.
11. Opila, E., Smialek, J., Robinson, R., Fox, D. and Jacobson, N., SiC recession caused by SiO_2 scale volatility under combustion conditions: II. Thermodynamics and gaseous-diffusion model. *J. Am. Ceram. Soc.*, 1999, **82**(7), 1826–1834.
12. Vaßen, R., Dietrich, M., Lehmann, H., Cao, X., Pracht, G., Tietz, F. *et al.*, Development of oxide ceramics for an application as TBC. *Mat. -wiss. u. Werkstofftech.*, 2001, **32**, 673–677.
13. Hannink, R. J., Kelly, P. M. and Muddle, B. C., Transformation toughening in zirconia-containing ceramics. *J. Am. Ceram. Soc.*, 2000, **83**(3), 461–487.
14. Lee, K. N., Fox, D. S. and Bansal, N. P., Rare earth silicate environmental barrier coatings for SiC/SiC composites and Si_3N_4 ceramics. *J. Eur. Ceram. Soc.*, 2005, **25**, 1705–1715.
15. Klemm, H., Fritsch, M. and Schenk, B., Corrosion of ceramic materials in hot gas environment. Proceedings of the 28th International Conference on Advanced Ceramics and Composites. *Ceram. Eng. Sci. Proc.*, 2004, **25**(4), 463–468.
16. Ueno, S., Jayaseelan, D., Kondo, N., Ohji, T. and Kanzaki, S., Corrosion mechanism of $Lu_2Si_2O_7$ phase in static state water vapor environment. Proceedings of the 28th International Conference on Advanced Ceramics and Composites. *Ceram. Eng. Sci. Proc.*, 2004, **25**(4), 451–455.